Photodissociation dynamics of the ethyl radical via the $\tilde{A}^2A'$ (3s) state: H-atom product channels and ethylene product vibrational state distribution

Ge Sun,[a] Xianfeng Zheng,[b] Yu Song,[c] Weidong Zhou,[d] and Jingsong Zhang*

Department of Chemistry

University of California at Riverside

Riverside, CA 92521

U.S.A.

Abstract

The photodissociation dynamics of jet-cooled ethyl radical (C_2H_5) via the $\tilde{A}^2A'(3s)$ state are studied in the wavelength region of 230-260 nm using the high-*n* Rydberg H-atom time-of-flight (HRTOF) technique. The H + C_2H_4 product channels are reexamined using the H-atom TOF spectra and photofragment translational spectroscopy. A prompt H + $C_2H_4(\tilde{X}^1A_g)$ product channel is characterized, with a repulsive translational energy release, anisotropic product angular distribution, and partially resolved vibrational state distribution of the $C_2H_4(\tilde{X}^1A_g)$ product. This fast dissociation is initiated from the 3s Rydberg state and proceeds via a H-bridged configuration directly to the H + $C_2H_4(\tilde{X}^1A_g)$ products. A statistical-like H + $C_2H_4(\tilde{X}^1A_g)$ product channel via unimolecular dissociation of the hot electronic ground-state ethyl ($\tilde{X}^2A'$) after internal conversion from the 3s Rydberg state is also examined, showing a modest translational energy release and isotropic angular distribution. An adiabatic H + excited triplet $C_2H_4(\tilde{a}^3B_{1u})$ product channel (a minor channel) is identified by energy-dependent product angular distribution, showing a small translational energy release, anisotropic angular distribution, and significant internal excitation in

the $C_2H_4(\tilde{a}^3B_{1u})$ product. The dissociation time of the different product channels are evaluated using energy-dependent product angular distribution and pump-probe delay measurements. The prompt H + $C_2H_4(\tilde{X}^1A_g)$ product channel has a dissociation time scale of < 10 ps, and the upper bound of the dissociation time scale of the statistical-like H + $C_2H_4(\tilde{X}^1A_g)$ product channel is < 5 ns.

a. Current address: Dalian Institute of Chemical Physics, Chinese Academy of Sciences, Dalian, Liaoning 116023, P. R. China.

b. Permanent address: Anhui Province Key Laboratory of Optoelectric Materials Science and Technology, Department of Physics, Anhui Normal University, Wuhu, Anhui 241000, P. R. China.

c. Permanent address: Beijing Academy of Quantum Information Sciences, Beijing, 100193, P. R. China.

d. Permanent address: Department of Optical Engineering and Key Laboratory of Optical Information Detection and Display Technology of Zhejiang, Zhejiang Normal University, Jinhua, Zhejiang 321004, P. R. China.

* Corresponding author. E-mail: jingsong.zhang@ucr.edu. Also at Air Pollution Research Center, University of California, Riverside, CA 92521.

Introduction

In hydrocarbon combustion processes, ethyl radical (C_2H_5) is an important intermediate.[1] The dissociation of ground electronic state ethyl radical to H atom and ethylene and its reverse reaction have been studied extensively by experiments and theories.[2-11] The dissociation of ethyl radical via the excited electronic states has also drawn considerable attentions.[12-22]

The UV absorption spectrum of the ethyl radical is comprised of broad and structureless bands due to Rydberg transitions.[23-27] The first absorption band is around 230-265 nm and peaks at 245 nm, corresponding to the $2p_z \rightarrow 3s$ [$\widetilde{X}^2A'$-$\widetilde{A}^2A'(3s)$] transition primarily on the α radical-center carbon atom. The second band in the region of 190-230 nm peaks around 206 nm and has been assigned to the $2p_z \rightarrow 3p$ excitation. The H-atom loss dissociation channels of the ethyl radical are listed as[28-30]

$$C_2H_5(\widetilde{X}^2A') \rightarrow H + C_2H_4(\widetilde{X}^1A_g) \quad \Delta H_0 = 34.91 \pm 0.06 \text{ kcal/mol} \quad (1)$$

$$\rightarrow H + C_2H_4(\tilde{a}^3B_{1u}) \quad \Delta H_0 = 96.83 \text{ kcal/mol} \quad (2)$$

$$\rightarrow H + CH_3CH(\text{triplet}, {}^3A'') \quad \Delta H_0 = 106.73 \pm 0.20 \text{ kcal/mol} \quad (3)$$

$$\rightarrow H + CH_3CH(\text{singlet}, {}^1A') \quad \Delta H_0 = 109.71 \pm 0.21 \text{ kcal/mol} \quad (4)$$

Figure 1 shows the energy level and correlation diagram of C_2H_5 photodissociation to the H atom and C_2H_4 products in C_s and C_{2v} symmetry. In the C_s symmetry, the ground-state ethyl $C_2H_5(\widetilde{X}^2A')$ correlates adiabatically with the H + ground-state $C_2H_4(\widetilde{X}^1A_g)$ products, and the excited-state $C_2H_5[\widetilde{A}^2A'(3s)]$ correlates adiabatically with H + excited-state $C_2H_4(\tilde{a}^3B_{1u})$. Theoretical studies have shown that upon excitation to the $\widetilde{A}^2A'(3s)$ Rydberg state from the ground-state $\widetilde{X}^2A'$ in the classical equilibrium geometry, one β H atom shifts towards the C-C bond center

into a non-classical H-bridged C_{2v} geometry (isomerization from $\tilde{A}^2A'(3s)$ in C_s to the lower energy $\tilde{A}^2A_1$ in C_{2v}).[12-14,22] In the C_{2v} symmetry, the ethyl $\tilde{A}^2A_1$ excited state correlates with the H + ground-state $C_2H_4(\tilde{X}^1A_g)$ products instead, and the H-bridged ground-state $C_2H_5(\tilde{X}^2B_2)$ correlates with the H + excited-state $C_2H_4(\tilde{a}^3B_{1u})$ on the $^2B_2$ surface. The $^2A_1$ and $^2B_2$ surfaces cross with a conical intersection (CI). Consequently, the ethyl radical excited to the $\tilde{A}^2A'(3s)$ state could migrate to the non-classical H-bridged structure, pass through the CI, and decompose into H and ground-state ethylene, via either a direct, fast dissociation (Channel 1a, with a large translational energy release) or an indirect dissociation after spending some time in the potential well of the ground-state ethyl radical (Channel 1b, with a small translational energy release).[13,14,22]

Previous experimental studies[18,21,22] on the photodissociation of ethyl via $\tilde{A}^2A'(3s)$ revealed bimodal product translational energy and angular distributions and thus two H-atom product channels: fast (high-kinetic energy E_T) H atoms with an anisotropic angular distribution and slow (low E_T) H atoms with an isotropic angular distribution, consistent with the dissociation pathways via the CI.[12-14,22] A recent direct *ab initio* molecular dynamics simulation of the ethyl $\tilde{A}^2A'(3s)$ photodissociation by Chen and co-workers confirmed that nonadiabatic dissociation via the CI produces the electronic ground-state ethylene and fast H atom products with an anisotropic angular distribution (Channel 1a in Figure 1), as well as hot ground-state ethyl that undergoes unimolecular dissociation to $C_2H_4(\tilde{X}^1A_g)$ + H with a small kinetic energy release (Channel 1b in Figure 1).[20] In addition, this work predicted an adiabatic dissociation pathway of the ethyl 3s Rydberg state to the electronic excited triplet ethylene $C_2H_4(\tilde{a}^3B_{1u})$ and H atom, with an anisotropic angular distribution (Channel 2 in Figure 1).[20] Selective β H-atom elimination was observed in the photodissociation of ethyl from the 3s Rydberg state by using partially-deuterated ethyl radicals.[15-18,21]

The dissociation rate of the H-atom product channels has been examined with both experimental and theoretical work.[17,20,21,31-34] The dissociation rate constants of ethyl via the $\tilde{A}^2A'(3s)$ state upon photoexcitation in the range of 264 to 245 nm were measured by Chen and co-workers to be ~10^6-10^7 s^{-1},[17] which were four to five orders of magnitude slower than the expected rate constant from the Rice-Ramsperger-Kassel-Marcus (RRKM) theory.[6,17] Fischer and co-worker measured the H-atom product kinetic energy distribution in the 250 nm photodissociation of ethyl as a function of pump and probe delay time, and showed a sub-nanosecond dissociation time constant for the H atoms with high E_T (Channel 1a) and confirmed a ~ 100 ns dissociation time for the low E_T H atoms (Channel 1b).[21] The classical trajectory calculations by Chen and co-workers showed that in the unimolecular dissociation of ethyl at a total energy of 120 kcal/mol, close to the UV photoexcitation energy at 238 nm, 78% trajectories dissociate to H + C_2H_4 in ~ 1 ps on the RRKM time scale, while the remaining hot ground-state ethyl radical is non-RRKM and persists with a lifetime > 7 ps, presumably trapped in long-lived quasiperiodic trajectories.[31,32] The more recent surface hopping trajectory calculations by Chen and co-workers followed the dissociation dynamics from the excited $\tilde{A}^2A'(3s)$ state and found that the direct dissociation of ethyl to H + ground-state C_2H_4 (Channel 1a) has a lifetime of ~ 30 fs, the indirect dissociation to H + ground-state C_2H_4 via the hot ground-state ethyl (Channel 1b) has a lifetime of ~ 2 ps, and the adiabatic dissociation from $\tilde{A}^2A'(3s)$ to H + $C_2H_4(\tilde{a}^3B_{1u})$ has a lifetime of ~ 100 fs.[20] It was then suggested that the previously observed unusually slow dissociation rate constant of ethyl[17] should arise from slow dissociation on the ground-state surface of ethyl.[20] A classical trajectory study of ethyl dissociation on the ground electronic state at the similar energy of 100-150 kcal/mol by Wagner and co-workers showed that ethyl dissociates in < 100 ps, consistent with the RRKM model, and there was no evidence of nanosecond lifetimes.[33] A roaming dissociation mechanism

of ethyl was also proposed to explain the unusually slow production of H atoms, in which the ethyl radical dissociates initially to vinyl radical + H_2 in a roaming pathway and the hot vinyl radical subsequently decomposes to H + C_2H_2 at a slow dissociation rate.[34] This slow H-atom production channel, however, would be a minor channel compared to H + C_2H_4, and furthermore it is energetically limited to low kinetic energy H atoms (e.g., E_T < 35 kcal/mol in the 245 nm photoexcitation).

In this paper, we report a further study on the photodissociation dynamics of jet-cooled ethyl radical via the $\tilde{A}^2A'(3s)$ state in the region of 230-260 nm by using the high-*n* Rydberg H-atom time-of-flight (HRTOF) technique. H-atom product TOF spectra were measured with linearly polarized photolysis laser radiation. The H-atom photofragment yield (PFY) spectrum (i.e. action spectrum) was obtained by integrating the H-atom TOF spectra at different photolysis wavelengths. From the H-atom TOF spectra at different photolysis laser polarizations, center-of-mass (CM) translational energy and angular distributions of the H + C_2H_4 products were derived. Two major H-atom loss dissociation channels were confirmed and further characterized: a prompt and anisotropic channel with a large, repulsive translational energy release and a statistical-like and isotropic one with a small translational energy release. A third, minor channel, with a prompt and anisotropic dissociation and a very small translational energy release, was observed for the first time and tentatively attributed to the electronic excited triplet state $C_2H_4(\tilde{a}^3B_{1u})$ + H products. These three dissociation channels are consistent with Channel 1a, 1b, and 2 in the direct *ab initio* molecular dynamics surface hopping trajectory calculations by Chen and co-workers.[20] With an improved resolution in the H-atom TOF spectra, vibrational state distribution of the ethylene product in the prompt, repulsive dissociation channel (Channel 1a) was partially resolved. The dissociation time scales of the H-atom products with different translational energies (i.e., in

different product channels) were examined by the H-atom angular distributions and by measuring the H-atom TOF spectra as a function of the pump-probe time delay. More insights into the photodissociation dynamics of ethyl [$\tilde{A}^2$A'(3s)] and the CI involved are provided.

Experimental

The experimental technique and apparatus of the high-*n* Rydberg H-atom time-of-flight (HRTOF) have been described in previous publications.[18,35-38] Nitroethane ($C_2H_5NO_2$, Aldrich 99.5%) and 3-pentanone ($C_2H_5COC_2H_5$, Aldrich > 99%) were employed as precursors to generate the ethyl radicals. The mixture of low-concentration precursors in Ar [0.2-2% (typically 0.2-0.5%)] at a total pressure of 1.2-1.5 atm was expanded from a pulsed nozzle. The pulsed ethyl radical beam was produced by photolyzing the precursors in front of the pulsed nozzle with a 193 nm radiation from an ArF excimer laser. The radicals formed from the photolysis were subsequently cooled by supersonic expansion and entrained in the seeded molecular beam (with rotational temperature of ~15−30 K).[39,40] The radical molecular beam was collimated by a skimmer downstream before entering the high vacuum interaction chamber. Further downstream in the photolysis region, the ethyl radicals were photodissociated by a tunable UV laser beam (at 230-260 nm, 0.2-1.8 mJ/pulse). The polarization of the photolysis radiation can be changed by a Fresnel-Rhomb achromatic λ/2 plate for the H-atom product angular distribution measurements. The H atoms formed from the photodissociation of the ethyl radicals were excited by two-color resonant excitation (121.6 nm + 366.3 nm), i.e., from 1^2S to 2^2P via the H-atom Lyman-α transition and then within 10 ns to a high-*n* Rydberg state. A small fraction of these metastable Rydberg H atoms drifted with their nascent velocities to a microchannel plate (MCP) detector that was positioned perpendicular to the molecular beam and were field-ionized in front of MCP and

detected. The nominal flight distance was 37.14 cm, which was calibrated by 236 nm photodissociation of HBr utilizing the well-studied HBr dissociation energy and the spin-orbit energy splitting of the Br($^2P_{3/2}$) and Br($^2P_{1/2}$) products. A fast pre-amplifier amplified the ion signals, and the signals were averaged by a multichannel scaler. The H-atom TOF spectra were typically accumulated with 60 to 180 k laser firings.

Results

1. H-atom TOF spectra, action spectrum, and products' translational energy and angular distributions

The ethyl radical beams using the nitroethane and 3-pentanone precursors were characterized by vacuum ultraviolet (VUV) single-photon ionization TOF mass spectrometry using the Lyman-α radiation at 121.6 nm. The production of the ethyl radicals (ionization energy 8.1 eV) from 193-nm photolysis of the precursors was identified at m/z 29 in the mass spectra. The H-atom product TOF spectra of the photodissociation of ethyl were measured in the photolysis wavelength region of 230-260 nm. Background in the TOF spectra, such as that from the precursors, was properly removed, as described in previous studies.[18,35-38] Figure 2 shows the net H-atom product TOF spectra of photodissociation of C_2H_5 (using nitroethane precursor) at 245 nm, with the UV photolysis radiation polarization parallel (∥, θ = 0°) and perpendicular (⊥, θ = 90°) with respect to the TOF axis. The H-atom TOF spectra using the 3-pentanone precursor were also taken and were similar, confirming that the ethyl radical was the common origin of the H-atom photodissociation signals. The photolysis laser power was kept mainly in the range of 0.5-1.8 mJ/pulse. A photolysis laser power dependence was examined at both parallel and perpendicular

polarizations, showing that the H-atom product signals in the entire TOF spectra had a linear power dependence in the photolysis laser power range of 0.5-1.8 mJ/pulse.

The H-atom PFY spectrum of the ethyl radical was obtained in the photolysis wavelength region of 230-260 nm (Figure 3). The spectrum was acquired by integrating the net H-atom TOF spectra of the ethyl radical photodissociation as a function of UV photolysis radiation wavelength. To correct for the variation and drift of the experimental conditions, the H-atom signals at 245 nm were taken as references and monitored after every 3 measurements at other wavelengths. The H-atom signal intensities at all photolysis wavelengths were normalized with the photolysis laser power and number of shots and then scaled to those at 245 nm. The H-atom PFY spectrum agrees well with the ethyl UV absorption spectrum by Fagerström *et al*,[25] providing further confirmation that the net H-atom signals were from photodissociation of the ethyl radical.

The net H-atom TOF spectra of the ethyl radical photodissociation are transformed to total center-of-mass (CM) translational energy distributions, $P(E_T)$'s. The CM translational energy of the products, E_T, is converted from the H-atom flight time t_H using the following equation:[41]

$$E_T = \left(1 + \frac{m_H}{m_{C_2H_4}}\right) E_H + \frac{m_H}{m_{C_2H_4}} E_{C_2H_5} = \frac{1}{2} m_H \left(1 + \frac{m_H}{m_{C_2H_4}}\right) \left(\frac{L}{t_H}\right)^2 + \frac{m_H}{m_{C_2H_4}} E_{C_2H_5} \qquad (5)$$

where E_T is the total CM translational energy of the H atom and ethylene products, E_H is the laboratory translational energy of the H-atom photofragment, and L is the flight length. The second term $\frac{m_H}{m_{C_2H_4}} E_{C_2H_5}$ is due to the parent C_2H_5 radical motion in the molecular beam which is orthogonal to the TOF path; and this term is very small compared with the first term. By using Equation (5), the $P(E_T)$ distributions of the H + C_2H_4 products at the 245 nm photodissociation wavelength with the linearly polarized photolysis radiation parallel ($\theta = 0°$, $P_{\parallel}(E_T)$) and perpendicular ($\theta = 90°$, $P_{\perp}(E_T)$) are derived from the corresponding H-atom TOF spectra in Figure

2 and are shown in Figure 4 (a) and (c), respectively. The product CM translational energy and photofragment angular distributions in the photodissociation can be related to the following equation:[42]

$$P(E_T, \theta) = \left(\frac{1}{4\pi}\right)[1 + \beta P_2(\cos\theta)]P(E_T) \quad (6)$$

where β is the anisotropy parameter (-1≤ β ≤2), θ is the angle between the electric vector of the linearly polarized photolysis radiation and the recoiling velocity vector of the H-atom product (the direction of detection or the TOF axis), $P_2(\cos\theta)$ is the second Legendre polynomial, and $P(E_T)$ is the angle-integrated translational energy distribution. The energy-dependent anisotropy parameter $\beta(E_T)$ is derived from Equation (6) and can be calculated by:[18]

$$\beta(E_T) = 2\frac{P_{\parallel}(E_T) - P_{\perp}(E_T)}{P_{\parallel}(E_T) + 2P_{\perp}(E_T)} \quad (7)$$

and $\beta(E_T)$ is shown in Figure 4 (d). The $P(E_T, \theta)$ at magic angle $\theta = 54.7°$, $P_m(E_T) = \frac{1}{4\pi}P(E_T)$, is calculated from $P_{\parallel}(E_T)$ and $P_{\perp}(E_T)$ and presented in Figure 4 (b).[42] $P_m(E_T)$ is independent of β and proportional to the angle-integrated $P(E_T)$; for convenience, $P_m(E_T)$ is used here to represent $P(E_T)$ for obtaining the product average translational energy release and the branching ratios.

2. Analysis of product channels in the products' translational energy and angular distributions

The $P(E_T)$ distributions show a bimodal distribution, while the anisotropy parameter $\beta(E_T)$ shows different value in three different regions. From E_T at the maximum available energy in the 245 nm photodissociation (81.76 kcal/mol) to about 65 kcal/mol, $\beta(E_T)$ stays near a constant

value of 0.67 ± 0.10. It gradually decreases to a constant value of ~ 0.0 ± 0.1 at E_T smaller than ~ 50 kcal/mol. When E_T is smaller than ~ 10 kcal/mol, $\beta(E_T)$ starts to increase and reaches a peak value of 0.25 ± 0.10 at ~ 2 kcal/mol in this low E_T region (corresponding to the 50-90 μs region in the TOF spectra in Figure 2). This behavior of the β parameter in the low E_T region is different from that of a typical statistical unimolecular dissociation, in which the β value is zero at low translational energy (for its dissociation time scale is longer than the parent rotational period). The accurate determination of the anisotropy parameter β requires reliable measurements of the H-atom TOF spectra at both parallel and perpendicular polarizations with proper background removal. The background in this system was broad and significant in the small E_T region, which could potentially cause larger uncertainty in the β value in the small E_T region. Nevertheless, with the improved instrument sensitivity and the signal averaging accumulated with large numbers of laser shots in multiple measurements (with total 360 k laser shots), the positive β value in the lowest energy region (E_T < 10 kcal/mol) was repeatedly observed, and the measured β value was considered to be reasonably reliable in this work.

The changing β parameter indicates at least three dissociation channels. The observed $P(E_T)$ can be considered to be the sum of the contributions from different dissociation channels, and the changing β value with E_T is due to the different β parameters for these different product channels and their energy-dependence branching ratios.[18,43] The overall product translational energy distribution, $P(E_T)$, and product translational energy-dependent anisotropy parameter, $\beta(E_T)$, can be expressed as $P(E_T) = P_{1a}(E_T) + P_{1b}(E_T) + P_2(E_T)$ and $\beta(E_T) = x_{1a}(E_T)\beta_{1a} + x_{1b}(E_T)\beta_{1b} + x_2(E_T)\beta_2$, where β_i is the anisotropy parameter of the *i*th product channel (assumed to be constant), $P_i(E_T)$ and $x_i(E_T)$ are the translational energy distribution and translational energy-dependent branching ratio of the *i*th product channel, $x_i(E_T) = \frac{P_i(E_T)}{P(E_T)}$, and

$x_{1a}(E_T)+x_{1b}(E_T)+x_2(E_T) = 1$. The product with anisotropic angular distribution ($\beta \sim 0.25$) and very small kinetic energy release at $E_T < 10$ kcal/mol is consistent with the high energy H + triplet $C_2H_4(\tilde{a}^3B_{1u})$ product channel (Channel 2 predicted by Chen and co-workers,[20] discussed more in the following). The maximum available energy of Channel 2 is 19.84 kcal/mol at the 245 nm photolysis wavelength,[28,30] and there is no contribution from Channel 2 at E_T larger than this threshold (i.e., $x_2(E_T) = 0$, at $E_T > 19.84$ kcal/mol). At $E_T > 19.84$ kcal/mol, $P(E_T)$ and $\beta(E_T)$ can be expressed as $P_{1a}(E_T) + P_{1b}(E_T)$ and $x_{1a}(E_T)\beta_{1a} + x_{1b}(E_T)\beta_{1b}$, respectively. As shown in the previous studies,[18] the β_{1b} parameter for the slow, isotropic unimolecular dissociation channel (Channel 1b) is 0, then $\beta(E_T) = x_{1a}(E_T)\beta_{1a}$ at $E_T > 19.84$ kcal/mol. $P_{1a}(E_T)$ for Channel 1a (the fast, anisotropic dissociation channel) is derived to be $\frac{2}{3\beta_{1a}}[P_{\parallel}(E_T) - P_{\perp}(E_T)]$. Assuming that near the maximum E_T, the contribution of Channel 1b is 0, then $x_{1a}(E_T) = 1$, $\beta_{1a} = 0.67 \pm 0.10$, and $P_{1a}(E_T)$ is readily derived. Similarly, at $E_T <$ ~50 kcal/mol, the contribution from Channel 1a is 0 and β_{1b} is 0, $\beta(E_T) = x_2(E_T)\beta_2$, and $P_2(E_T)$ for Channel 2 (the low E_T, anisotropic dissociation channel) can be expressed as $\frac{2}{3\beta_2}[P_{\parallel}(E_T) - P_{\perp}(E_T)]$. Depending on the maximum $x_2(E_T)$ value in the lowest energy region, β_2 is in the range of 0.25 ± 0.10 to 2. The anisotropic parameter β of the $C_2H_4(\tilde{a}^3B_{1u})$ + H channel (Channel 2) was predicted to be ~1.3 by Chen and co-workers;[20] assuming this value for β_2, $P_2(E_T)$ can then be derived. Thus, the $P(E_T)$ is deconvoluted into $P_{1a}(E_T)$, $P_{1b}(E_T)$, and $P_2(E_T)$, for the three dissociation channels, Channel 1a, Channel 1b, and Channel 2, respectively, as shown in Figure 4 (b). In the 245 nm photodissociation of ethyl, the average translational energy release of these three dissociation channels, $\langle E_T \rangle$, are estimated to be 63.9, 22.2, and 3.6 kcal/mol, respectively. The fraction of $\langle E_T \rangle$ of the three dissociation channels in the total available energy to the H + $C_2H_4(\tilde{X}^1A_g)$ products, $\langle f_T \rangle$, are 0.78, 0.27, and 0.04 [or 0.18

to the H + $C_2H_4(\tilde{a}^3B_{1u})$ products for Channel 2], respectively. The branching ratios of the three dissociation channels are calculated to be 0.11:0.87:0.02. Note that depending on the assumed β_2 value, the contribution of Channel 2 could be from 0.01 (for β_2 = 2) to 0.10 (for β_2 = 0.25); nevertheless, Channel 2 is a minor channel, with the smallest branching fraction. With its small branching ratio and the uncertainty, the above derived $P_2(E_T)$ is considered as tentative evidence of the H + $C_2H_4(\tilde{a}^3B_{1u})$ product channel. The $\langle E_T \rangle$, $\langle f_T \rangle$, β parameter, and branching ratios for each dissociation channel are summarized in Table 1.

3. Analysis of vibrational state distribution of the $C_2H_4(\tilde{X}^1A_g)$ product in Channel 1a

In this study, the energy resolution in the $P(E_T)$ distribution was improved by using very diluted precursors (~ 0.5%) in Ar and better cooling of the radicals in the seeded molecular beam, and the detection sensitivity was also improved to achieve a good signal to noise (S/N) ratio. As shown in Figure 2 (a) and Figure 4 (a), some fine structures are apparent in the anisotropic, high translational energy region (E_T > 60 kcal/mol), indicating partially resolved vibrational state distribution of the ethylene product in Channel 1a. As described above, the product CM translational energy distribution for Channel 1a, $P_{1a}(E_T)$, is obtained as $\frac{2}{3\beta_{1a}}[P_{\parallel}(E_T) - P_{\perp}(E_T)]$ and shown in Figure 4 (b). The available energy is distributed to the translational, vibrational, and rotational energy in the products. The maximum translational energy released is determined by the photolysis energy and the C-H bond dissociation energy which corresponds to the $C_2H_4(\tilde{X}^1A_g)$ product. The internal energy distribution $P_{1a}(E_{int})$ of the $C_2H_4(\tilde{X}^1A_g)$ product in the repulsive Channel 1a is then derived from the $P_{1a}(E_T)$ distribution and shown in Figure 5.

The internal energy distribution $P_{1a}(E_{\rm int})$ peaks around 6000 cm^{-1} (17 kcal/mol), showing a significant internal (predominantly vibrational) excitation of the $C_2H_4(\tilde{X}^1A_g)$ product in Channel 1a, despite the repulsive translational energy release. Also, the $P_{1a}(E_{\rm int})$ distribution has a good S/N ratio at $E_{\rm int}$ < 6500 cm^{-1} (at E_T > 60 kcal/mol) and shows some partially resolved vibrational structure of C_2H_4. The vibrational normal modes and vibrational frequencies of ethylene have been well studied.[44-48] The 12 normal modes of C_2H_4 can be grouped into 4 categories: C-C stretching (ν_2), C-H stretching (ν_1, ν_5, ν_9, and ν_{11}), H-C-H in-plane bending (ν_3, ν_6, ν_{10}, and ν_{12}), and H-C-H out-of-plane torsion or bending (ν_4, ν_7, and ν_8). The ν_7 and ν_8 modes are nearly identical with close vibrational frequencies and can be treated as one mode. In the direct, repulsive dissociation Channel 1a, ethyl (with an equilibrium C-C single bond distance of 1.52 Å[14]) is excited to the Franck-Condon region of the 3s Rydberg state that evolves to the CI region in C_{2v} symmetry and then dissociates to the $C_2H_4(\tilde{X}^1A_g)$ product (with a shorter equilibrium C=C double bond distance of 1.339 Å[49]), and thus the C-C stretching vibration (ν_2) is expected to be excited in the ethylene product. The H-C-H out-of-plane torsion and bending of the C_2H_4 product could also be excited in going from a non-planar H-C-H moiety in ethyl to a planar one in C_2H_4. C-H stretching motion in C_2H_4 should be minimal, as the lengths of the C-H bonds essentially do not change during the dissociation process, except for the cleaved C-H bond. To qualitatively model the vibrational state distributions of the $C_2H_4(\tilde{X}^1A_g)$ product, $P_{1a}(E_{\rm int})$ is fitted with multiple Gaussian peaks with adjustable height, position, and width as shown in Figure 5.

In the fitting/modeling process, the positions of the vibrational peaks of $C_2H_4(\tilde{X}^1A_g)$ were calculated based on vibrational frequencies and anharmonicities in Herman's work.[48] The ν_2 progression was added first and found to be insufficient for filling the structures in $P(E_{\rm int})$, indicating that other vibrational modes are also excited in the ethylene product. In the small internal

energy region ($<$ 1600 cm^{-1}), several fundamental vibrational modes (ν_{10} ~ 770 cm^{-1}, ν_7/ν_8 ~ 940 cm^{-1}, ν_4 ~ 1080 cm^{-1}, ν_6 ~ 1250 cm^{-1}, ν_3 ~ 1340 cm^{-1}, ν_{12} ~ 1440 cm^{-1}, and ν_2 ~ 1600 cm^{-1}) were assigned with little ambiguity, and they match with the observed structures. Next peak around 1750 cm^{-1} was assigned to $\nu_7/\nu_8 + \nu_{10}$ combination vibrational motion. Similarly, the overtone and combination vibrational states of the above low frequency modes were added with increasing energy. The C-H stretching (ν_1, ν_5, ν_9, and ν_{11}) peaks, with a large separation of ~ 3000 cm^{-1}, were sparce and of minimal intensity. The first half of the $P(E_{\text{int}})$ distribution (E_{int} < 6500 cm^{-1}), with a good S/N, was filled with around 50 peaks and then signed to different vibrational modes. Adjustments on position, width, and intensity were made if necessary to fit both the experimental data and prediction of the positions for E_{int} < 6500 cm^{-1}. The width of the peaks was determined by the instrumentation energy resolution and the rotational excitation in the ethylene product. These peaks are mainly assigned to five pure vibrational mode progressions: ν_2, ν_4, ν_6, ν_7/ν_8, and ν_{12}, as well as combination mode progressions such as $\nu_7 + \nu_{12}$, $\nu_6 + \nu_{12}$, $\nu_7 + \nu_2$ *et al.*, which are needed to reproduce the $P(E_{\text{int}})$ distribution. Apparently, C-C stretching, in-plane H-C-H bending, and out-of-plane H-C-H bending are primarily excited in the $C_2H_4(\tilde{X}^1A_g)$ product from C_2H_5 photodissociation. The C-H stretching progression has smaller intensities and larger uncertainty. In the large internal energy region ($>$ 6500 cm^{-1}), the vibrational peak positions were calculated based on the vibrational frequencies and anharmonicities of C_2H_4 and extension of the vibrational progressions from the lower energy region (< 6500 cm^{-1}). The $P(E_{\text{int}})$ distribution has a lower S/N ratio at E_{int} > 6500 cm^{-1}, and it was modelled (instead of fitted) using the estimated peak positions with the peak widths and intensities adjusted if necessary. The peak assignments of the ethylene product in this region were more ambiguous, and the modelled vibrational distribution was only qualitative and may not be unique. Overall, it is concluded from the above modeling that many of

the vibrational modes in the $C_2H_4(\tilde{X}^1A_g)$ product in Channel 1a are excited, especially the C-C stretching (ν_2) and H-C-H bending modes. Possible/tentative peak assignments are listed in Figure 5, and the information of the major progressions are summarized in Table 2.

4. Pump-probe measurements of dissociation rate constant

The H-atom product yield time profile in the UV photodissociation of ethyl radical was studied by measuring the HRTOF spectra as a function of delay time between the photolysis laser (pump laser) and probe laser beams. Both precursors, nitroethane and 3-pentanone, were used in this study and showed identical results. The H-atom TOF spectra of the photodissociation of ethyl (from the nitroethane precursor) at 244 nm with different pump-probe delay time are shown in Figure 6. The signals of the H-atom TOF spectra reached the maximum at 10 ns pump-probe delay time and then decreased monotonically with the increasing delay time. The H-atom product yield time profiles for the 244 nm photodissociation of ethyl (with the nitroethane precursor) are shown in Figure 7. The time profiles were obtained by integrating the H-atom product signals in the HRTOF spectra in different TOF windows as a function of the pump-probe delay time and were scaled to the maximum for each time profile. The different TOF windows in the H-atom TOF spectra (the total H atoms, fast H atoms from Channel 1a, and slow H atoms from Channel 1b) were integrated to check any possible bias on the H-atom time profile due to the flyout of the H atoms from the interaction region and the H atoms formed from the different dissociation channels. These three time profiles from the different TOF or E_T windows have essentially the same rise time of ~ 10 ns (approaching the limit of the laser temporal resolution), but different decay time after the peak due to the different velocities of the H atoms flying out of the interaction region.

The pump-probe delay time profiles provide a measure of the microcanonical rate constant of the unimolecular dissociation of the ethyl radical. The rise of the signals in the 0 to 10 ns early

delay time region indicates the formation of H-atom product from the ethyl radical, while the decay of the signals after the peak is due to H-atom flight out of the interaction region between the photolysis and probe radiations. The H-atom product from the unimolecular dissociation of the ethyl radical can be described by the following expression:[17,39]

$$S_H(t) = N[1 - \exp(-k_H t)] \cdot \frac{1}{\exp\left[\frac{t-a}{b}\right]+1} \quad (8)$$

where $S_{\mathrm{H}}(t)$ is the time profile of the H-atom signals, k_{H} is the unimolecular dissociation rate constant of the ethyl radical, and a and b are the constants to describe the width of the plateau region and the decay of the signals. The fittings in Figure 7 indicate the dissociation rate constant of $k_{\mathrm{H}} \sim 2 \times 10^8$ s^{-1} for all three time profiles in the 244 nm photodissociation of ethyl (using the nitroethane precursor). The measurements using the 3-pentanone precursor (not shown here) give identical results. The 10-ns time resolution of the pump and probe laser radiations limits the H-atom product appearance time resolution, then the k_{H} value gives the lower limit of the actual dissociation rate constant.

The reliability of the measurements of the H-atom production rate constant of ethyl can be confirmed by similar measurements on systems with well-known dissociate rate constants using the same instrument. The H-atom product time profiles of UV photodissociation of HBr and SH in the range of 220-240 nm, which are on sub-picosecond time scales, showed a 10-ns rise time that is limited by the 10-ns time resolution of the laser radiations, similar to ethyl. On the other hand, our earlier work on the photo-predissociation of the OH radical in $A^2\Sigma^+$ ($v' = 2, J' = 2.5$) state measured a dissociation rate constant of $k_{\mathrm{H}} \approx 7.7 \times 10^6$ s^{-1} with a dissociation time scale of 130 ± 30 ns,[50] in excellent agreement with the previous experimental value of 130 ± 10 ns.[51] Furthermore, our previous work on the photo-predissociation of the SD $A^2\Sigma^+$ ($v' = 0, J' = 1.5$) state determined

a dissociation rate constant of $k_H \approx 4.05 \times 10^6$ s^{-1} with a dissociation time scale of 247 ± 50 ns,[52] in excellent agreement with the previous experiments.[53] Both confirm that our experimental method can actually measure slow production of H-atom products (in > 10 ns time scale) from the dissociation of ethyl if they were present. It is also noted that the D-atom product in the SD case has an E_T < 4 kcal/mol and the H-atom product in the OH case < 7 kcal/mol, indicating that the low E_T products can be efficiently and accurately characterized in our experiment.

Discussion

The overall behaviors of the product translational energy distribution $P(E_T)$ and angular distribution $\beta(E_T)$ of the UV photodissociation of ethyl via the $\widetilde{A}^2A'$ (3s) Rydberg state in this study are consistent with our previous experiment work[18] and other recent ones by Fischer with co-workers and Bañares with co-workers,[18,21,22] as well as the recent surface hopping trajectory calculation by Chen and co-workers.[20] The high E_T H + $C_2H_4(\widetilde{X}^1A_g)$ product channel, with $\langle f_T \rangle \sim 0.78$ and $\beta \sim 0.67 \pm 0.10$, is the same as the one observed previously, with $\langle f_T \rangle \sim 0.78$ and $\beta = 0.5 \pm 0.1$ from our earlier work[18] and similar values from other recent studies.[21,22] This fast and anisotropic product channel is consistent with the direct C-H bond cleavage across CI via a nonclassical H-bridged configuration from the 3*s* Rydberg excited state.[12-14,22,18] This large E_T and anisotropic channel is also identified in the theoretical study by Chen and co-workers, as Channel 1a, with $\langle f_T \rangle \sim 0.85$ and $\beta \sim 0.8$.[20] The low E_T and isotropic H + $C_2H_4(\widetilde{X}^1A_g)$ product channel, with $\langle f_T \rangle \sim 0.27$ and $\beta \sim 0.0 \pm 0.1$, is the same as the slow one observed previously, with $\langle f_T \rangle \sim 0.35$ and $\beta \sim 0.0 \pm 0.15$ from our earlier work[18] and similar values from others.[21,22] This channel corresponds to the unimolecular dissociation of the internally hot radical on the ground electronic

state after internal conversion via CI in C_{2v} geometry from the 3*s* excited state.[18] This slow, isotropic channel is also identified in the surface hopping trajectory study by Chen and co-workers, as Channel 1b, with $\langle f_T \rangle \sim 0.36$ and $\beta \sim 0$.[20] The branching ratio between Channel 1a and 1b was measured to be ~ 0.13:1, similar to the value of ~ 0.2:1 from our earlier work[18] and to values from other studies that also showed predominant production of Channel 1b.[21,22] This compares with the branching ratio of 0.19 from the theoretical study by Chen and co-workers.[20] Furthermore, the surface hopping trajectory calculation by Chen and co-workers predicted a direct, adiabatic dissociation channel of the ethyl $\tilde{A}^2A'$ (3s) to the high-energy H + $C_2H_4(\tilde{a}^3B_{1u})$ products (with a small $\langle f_T \rangle \sim 0.29$ and ~ 0.15 fraction of the total dissociation (which highly depends on the potential energy surfaces used in the calculations], as Channel 2.[20] Our current experiment observed the anisotropic product channel ($\beta = 0.25 \pm 0.10$ to 2, more details in the following) with very small translational energy release [$\langle E_T \rangle \sim 3.6$ kcal/mol and $\langle f_T \rangle \sim 0.18$ with respect to the H + $C_2H_4(\tilde{a}^3B_{1u})$ products], consistent with this triplet ethylene $C_2H_4(\tilde{a}^3B_{1u})$ + H product channel (Channel 2). This would be the first experimental observation of this product channel, although it is a minor channel with a small branching ratio (~ 0.02) among the three product channels.

1. Channel 1a

The Channel 1a component peaks at ~ 65 kcal/mol with $\langle f_T \rangle \sim 0.78$ and an anisotropic angular distribution with $\beta \sim 0.67 \pm 0.10$ in the 245-nm photodissociation, consistent with our previous photodissociation study of the ethyl radical,[18] other recent experimental studies,[21,22] and the theory by Chen and co-workers.[20] The pump-probe delay study implies that the dissociation time scale is shorter than ~ 5 ns, and the anisotropic angular distribution indicates that the dissociation time scale of this high E_T channel is shorter than one rotational period of the ethyl

parent molecule (~ 10 ps). This dissociation time scale is consistent with the theoretical value of ~ 30 fs from the surface hopping trajectory calculations by Chen and co-workers for direct dissociation of the excited $\tilde{A}^2A'(3s)$ state to H + ground-state $C_2H_4(\tilde{X}^1A_g)$ via the CI (Channel 1a). The dissociation mechanism of Channel 1a is the prompt, direct dissociation of the ethyl radical on the electronic excited state via the CI in C_{2v} symmetry and then produces the fast H-atom and $C_2H_4(\tilde{X}^1A_g)$ with an anisotropic angular distribution (see Figure 1).

The $C_2H_4(\tilde{X}^1A_g)$ product in Channel 1a is vibrationally excited. In the direct, repulsive dissociation, the $C_2H_4(\tilde{X}^1A_g)$ product with the C=C double bond is formed after ethyl is excited to the Franck-Condon region of the 3*s* Rydberg state that evolves to the CI region and then dissociates to the $C_2H_4(\tilde{X}^1A_g)$ product, with a shortening of the C-C bond distance from 1.52 Å in ethyl[14] to 1.339 Å in ethylene.[49] The C-C stretching vibration (ν_2) of C_2H_4 is excited. The H-C-H out-of-plane and in-plane bending modes of the C_2H_4 product are also excited in going from a non-planar H-C-H moiety in ethyl to a planar one in C_2H_4. Assuming in the prompt dissociation a sudden departing of the H atom near the CI region, the C-C bond distance before the breaking of the C-H bond can be simulated using a simple one-dimensional Franck-Condon modeling that is performed based on the fitted vibrational population of the ν_2 progression (C-C stretch). In the modeling, Morse oscillator is used to simulate the C-C stretching in ethylene, and a harmonic oscillator on ground vibrational state is applied for the C-C stretching of the excited ethyl radical just prior to the prompt dissociation. To simplify the vibrational model, the CH_2 or CH_3 group in ethylene and ethyl radical are treated as rigid bodies without the relative C-H motions. The Franck-Condon relative population distribution of the C-C stretching of the ethylene product can be calculated by projecting the C-C stretching wavefunction of the excited ethyl radical onto the basis set of the ethylene C-C stretching vibration. During the calculation, the excited ethyl radical C-C stretching

frequency and C-C bond distance (used as the equilibrium distance in the harmonic oscillator) are adjusted until a best fit of the experimental ethylene C-C stretching intensities is achieved. The parameters for ethylene are based on works from the Herman and Ramsay groups,[48,49] with R_{eq} (C-C) = 1.339 Å, ν_2 (C-C stretching frequency) = 1634.00 cm^{-1}, and $\chi_{2,2}$ (C-C stretching anharmonicity parameter) = -2.46 cm^{-1}. When ν (C-C) ≈ 2060 cm^{-1} and R_{eq} (C-C) ≈ 1.51 Å for the excited ethyl radical, the simulation reached the best fit of the ethylene C-C stretching vibrational progression (shown in Figure 8).

From the Franck-Condon modeling, the C-C bond distance of the $\tilde{A}^2A_1$ state ethyl when the C-H bond breaks is essentially the same as the equilibrium R_{eq} (C-C) of the ground-state ethyl radical (1.52 Å calculated at the CASSCF level by Zyubin et al.),[14] and thus the same C-C distance in the Franck-Condon region of the excited $\tilde{A}^2A'(3s)$ state upon the photoexcitation. This C-C distance is shorter than the calculated value of 1.56 Å at the minimum energy crossing point in the CI region in C_{2v},[14] suggesting that H-atom migration from the classical geometry in the Franck-Condon region to the H-bridged geometry in C_{2v} and the subsequent repulsive dissociation to H + $C_2H_4(\tilde{X}^1A_g)$ take place rapidly before the C-C bond distance can change. This is consistent with the ~ 30 fs dissociation time scale of Channel 1a from the surface hopping trajectory calculations by Chen and co-workers,[20] which is close to the C-C vibrational period of ~ 25 fs and thus gives little time for the C-C bond to change. The highly excited H-C-H out-of-plane bending (ν4 and ν7/ν8, up to 10 and 12 quanta and with the most intense peak with 7 quanta for both modes) of the ethylene product indicates that these six atoms are not on the same plane or even far away from a planar structure when the β H-atom elimination occurs. Related to this, the H-C-H in-plane bending (ν_3, ν_6, ν_{10}, and ν_{12}) is also excited. Overall, the prompt C-H bond breaking occurs from the H-bridged configuration on the $\tilde{A}^2A_1$ state while the rest of the ethyl radical has a similar

geometry to that in the Franck-Condon region of the $\widetilde{A}^2A'(3s)$ state (i.e., the equilibrium geometry of the ground state ethyl).

The partially resolved vibrational structure of $C_2H_4(\widetilde{X}^1A_g)$ in the $P(E_T)$ distribution of Channel 1a suggests that the rotational excitation of the $C_2H_4(\widetilde{X}^1A_g)$ product is small (relatively narrow vibrational peaks). Based on conservation of angular momentum, in the dissociation of jet-cooled ethyl (with nearly zero initial rotational angular momentum), the small rotational excitation in the C_2H_4 product relates to small orbital angular momentum of the departing H atom and thus small impact parameter. The small impact parameter would be consistent with the C_{2v} dissociation geometry via CI for Channel 1a, where the H-atom departs near the H-bridged position on the C_{2v} axis or close to the center of mass of the C-C bond.

2. Channel 1b

The product formed in Channel 1b has a modest translational energy release ($\langle f_T \rangle \sim 0.27$). The angular distribution of the H-atom produced from Channel 1b in Figure 4 shows an isotropic distribution. Channel 1b is consistent with unimolecular dissociation of hot ethyl radical in the ground electronical state after internal conversion from the initially excited 3s Rydberg state via the CI (Figure 1). The isotropic distribution indicates that the dissociation time scale of Channel 1b should be equal or longer than one rotational period of the ethyl radical (~ 10 ps), thus an upper limit of the dissociation rate constant of ~ 10^{11} s^{-1}. The pump-probe experiment in this study provided a lower limited of the dissociation rate constant with 2×10^8 s^{-1} at 244 nm photolysis wavelength, limited by the 10 ns laser resolution.

The early experimental study on the unimolecular dissociation rate constant of ethyl via the $\widetilde{A}^2A'(3s)$ state by Chen and co-workers measured an ethyl dissociation rate constant of 1.8 ×

10^7 s^{-1} at 250 nm (114 kcal/mol) excitation.[17] Fischer and co-worker confirmed a ~ 100 ns dissociation time for the low E_T H atoms (Channel 1b) in the 250 nm photodissociation of ethyl.[21] The precious RRKM study of Hase *et. al.* indicated that at a 100 kcal/mol excitation energy, the dissociation rate constant is 1.7×10^{11} s^{-1},[6] about 4 orders of magnitude faster. And the classical trajectory study of ethyl dissociation on the ground electronic state at the similar energy of 100-150 kcal/mol by Wagner and co-workers also indicated that ethyl dissociates in < 100 ps.[33] The surface hopping trajectory calculations by Chen and co-workers showed that the indirect dissociation to H + ground-state C_2H_4 via the hot ground-state ethyl (Channel 1b) has a time constant of ~ 2 ps,[20] and suggested that the previously observed unusually slow dissociation rate constant of ethyl[17] should arise from slow dissociation on the ground-state surface of ethyl. In our current study at the 244 nm photolysis wavelength, the dissociation rate constant of both the high E_T and low E_T channels are measured to be > 2×10^8 s^{-1} (limited by the 10-ns laser temporal resolution), which is at least 10 times faster than those measured at the similar excitation energies by Chen and co-workers[17] and Fischer and co-worker.[21] The lower limit of the dissociation rate constant measured in this study is more consistent with the RRKM, classical trajectory, and surface hopping trajectory calculations on the unimolecular dissociation of ethyl radical. Our dissociation rate constant measurements do not support the roaming dissociation mechanism of ethyl that produces H atoms at a slow dissociation rate,[34] as argued in the Introduction section.

It is also noted that site-selective β H-atom elimination has been observed in the UV photodissociation of isotope-labeled ethyl (CD_3CH_2) via the 3s Rydberg state.[15-18,21] This would imply that unimolecular dissociation of ethyl on the ground electronic state following the internal conversion from the excited state takes place in a short time, which prevents H/D atom scrambling on the hot ground electronic state of ethyl prior to the dissociation.

3. Channel 2

Chen and co-workers' surface hopping trajectory calculations predicted an adiabatic dissociation channel of the ethyl radical on the $\tilde{A}^2A'$ state that leads to the H + $C_2H_4(\tilde{a}^3B_{1u})$ products with an anisotropy angular distribution and a very small translational energy release.[20] The theoretical study also showed that this direct adiabatic dissociation from $\tilde{A}^2A'(3s)$ to H + $C_2H_4(\tilde{a}^3B_{1u})$ has a timescale of ~ 100 fs.[20]

In Figure 4 (c), the anisotropy parameter β increases from 0 and reaches the maximum value of ~ 0.25 when the CM translational energy decreases from 10 kcal/mol to ~ 2-3 kcal/mol. The changing β indicates that there are at least two dissociation channels in this translational energy region. Channel 1b, the unimolecular dissociation of the ethyl radical after the internal conversion from the 3s Rydberg state that leads to the H + $C_2H_4(\tilde{X}^1A_g)$ products with an isotropic angular distribution and modest translational energy in this region, is one of the product channels, as discussed above and studied previously.[13,14,18,20,21,22] The positive β here suggests another prompt and direct dissociation channel from the excited state of ethyl to the H + C_2H_4 products, with a dissociation time scale shorter than one rotational period of the ethyl radical. The methylene H-atom elimination channel of ethyl, H + CH_3CH, would have a very small E_T release, but the experimental observation of the site-selective β H-atom elimination in the UV photodissociation of ethyl via the 3*s* state[13,14,18,20,21] disproves this product channel. Furthermore, in the prompt dissociation with an anisotropic angular distribution, the methylene H-atom elimination channel is expected to have a negative β parameter as the transition dipole moment is perpendicular to the methylene plane and thus the velocity vector of the departing H atom; thus the observed positive β value further rules out the α-H elimination channel. The very low CM translational energy for this product channel is consistent with the high energy H + triplet ethylene $(\tilde{a}^3B_{1u})$ product channel.

Similar to the treatment for Channel 1a, the product CM translation energy distribution for Channel 2, $P_2(E_T)$, is proportional to $P_{\parallel}(E_T) - P_{\perp}(E_T)$. The observed average translational energy, $\langle E_T \rangle$, for Channel 2 is calculated to be ~ 3.6 kcal/mol, and the small translational energy release ($\langle f_T \rangle$ ~ 0.18) indicates an internally excited ethylene product. To estimate the anisotropy parameter for Channel 2, the $P_{1b}(E_T)$ is calculated to be $\frac{1}{3} \times (P_{\parallel}(E_T) + 2 \times P_{\perp}(E_T)) - \frac{1}{\beta_2} \times \frac{2}{3} \times (P_{\parallel}(E_T) - P_{\perp}(E_T))$. With the constrained condition that $P_{1b}(E_T)$ and $P_2(E_T)$ are larger than 0, the β_2 value is determined to be in the range of 1.0 to 2.0.

The dissociation mechanism of Channel 2 would be the direct β-CH bond cleavage in the C_S plane. The transition dipole momentum $\boldsymbol{\mu}$ of the initial $\widetilde{A} \leftarrow \widetilde{X}$ transition lies in the C_S mirror plane of the ethyl radical and perpendicular to the C-C bond. If the leaving β H atom departs along the cleaving C-H bond in its equilibrium geometry in ethyl, the angle between $\boldsymbol{\mu}$ and the velocity of the H atom is ~ 22° and would give rise a anisotropy parameter of ~ 1.5, which is consistent with the prediction by Chen and co-workers.[20] As shown in Figure 1, the dissociation pathway in Channel 2 can be viewed as a direct dissociation of C_2H_5 $\widetilde{A}^2A'$ to its adiabatically correlated H + $C_2H_4(\tilde{a}^3B_{1u})$ products. Alternatively, this pathway could be viewed as some minor amount of dissociation flux from $\widetilde{A}^2A_1$ in the C_{2v} geometry skipping the CI region and surface hopping, leading adiabatically to the excited H + $C_2H_4(\tilde{a}^3B_{1u})$ products instead of the ground-state H + $C_2H_4(\widetilde{X}^1A_g)$ products.

The structure of the $C_2H_4(\tilde{a}^3B_{1u})$ has been study theoretically,[30,54,55] and $C_2H_4(\tilde{a}^3B_{1u})$ was also observed experimentally in the UV photodissociation of ethylene sulfide.[56] At equilibrium, the two CH_2 planes in $C_2H_4(\tilde{a}^3B_{1u})$ are perpendicular (φ = 90°) to each other in a D_{2d} symmetry group, with an elongated C-C bond than the planar ground-state $C_2H_4(\widetilde{X}^1A_g)$. The direct, prompt

cleavage of the CH bond in the excited ethyl to form the triplet C_2H_4, however, would create the C_2H_4 product in a nearly planar structure, far away from the equilibrium geometry of the triplet $C_2H_4(\tilde{a}^3B_{1u})$ and thus with a significant vibrational excitation. Our observation on this anisotropic channel also indicates that the translational energy release of the H + $C_2H_4(\tilde{a}^3B_{1u})$ products is much smaller than the maximum available energy, and the remaining available energy should be distributed in the internal modes of the triplet ethylene product.

In conclusion, the H atom + triplet $C_2H_4(\tilde{a}^3B_{1u})$ product channel is observed from the photodissociation of ethyl via the $\tilde{A}^2A'$ state for the first time. This dissociation pathway would be an adiabatic dissociation along the potential energy surface in the C_{2v} symmetry skipping the CI region with the surface hopping, and the cleavage of the CH bond in the H-bridged configuration creates the H + excited triplet $C_2H_4(\tilde{a}^3B_{1u})$ products with a positive anisotropy parameter and significant internal excitation in the ethylene product.

Conclusion

The reinvestigation of UV photodissociation dynamics of ethyl radical via the $\tilde{A}^2A'(3s)$ Rydberg state by HRTOF provides additional information about the β H-atom elimination mechanism. The repulsive, prompt dissociation is initiated from the 3*s* Rydberg state and proceeds via a H-bridged configuration through the CI in C_{2v} geometry to the H + $C_2H_4(\tilde{X}^1A_g)$ product (Channel 1a), with a large translational energy released ($\langle f_T \rangle \sim 0.78$) and anisotropic product angular distribution ($\beta \sim 0.67 \pm 0.10$). The ethylene product vibrational state distribution in Channel 1a is obtained, and the Franck-Condon calculation is performed to determine some geometry information of the ethyl radical before the H-atom elimination. A statistical-like H +

$C_2H_4(\tilde{X}^1A_g)$ product channel (Channel 1b) proceeds via the unimolecular dissociation of the hot ground state ethyl radical after internal conversion from the 3s Rydberg state through the CI in C_{2v}, with a modest translational energy release ($\langle f_T \rangle \sim 0.27$) and isotropic product angular distribution ($\beta \sim 0.0 \pm 0.1$). A high-energy H + triplet $C_2H_4(\tilde{a}^3B_{1u})$ product channel (Channel 2) is observed experimentally for the first time, with a small translation energy release ($\langle E_T \rangle \sim 3.6$ kcal/mol and $\langle f_T \rangle \sim 0.18$), highly internally excited $C_2H_4(\tilde{a}^3B_{1u})$ product, and anisotropic product angular distribution ($\beta \sim 1.0$-2.0). This channel is an adiabatic dissociation channel of the ethyl 3*s* state, where the dissociation flux skips through the CI region in the C_{2v} symmetry and undergoes surface hopping to the H + triplet $C_2H_4(\tilde{a}^3B_{1u})$ product channel. The product branching ratios are determined to be 0.11:0.87:0.02 for these three channels, respectively. The energy-dependent product angular distribution and pump-probe delay measurements of the H-atom signals indicate that the prompt H + $C_2H_4(\tilde{X}^1A_g)$ product channel has a dissociation time scale of < 10 ps, and the upper bound of the dissociation time scale of unimolecular dissociation to the H + $C_2H_4(\tilde{X}^1A_g)$ products is < 5 ns. The latter is consistent with the previous RRKM and trajectory calculations.

Acknowledgement

This work was supported by the US National Science Foundation (grant number CHE-2155232) and a UC MEXUS-CONACYT Collaborative Grant (CN-16-68).

Conflict of interest

The authors have no conflicts to disclose.

Reference

1. J. Warnatz, *Combustion Chemistry* (Springer New York, 1984).
2. W. Tsang and R. F. Hampson, *J. Phys. Chem. Ref. Data* **15**, 1087 (1986).
3. Y. Feng, J. T. Niiranen, A. Bencsura, V. D. Knyazev, D. Gutman, and W. Tsang, *J. Phys. Chem.* **97**, 871 (1993).
4. P. D. Lightfoot and M. J. Pilling, *J. Phys. Chem.* **91**, 3373 (1987).
5. W. L. Hase, G. Mrowka, R. J. Brudzynski, and C. S. Sloane, *J. Chem. Phys.* **69**, 3548 (1978).
6. W. L. Hase, R. J. Wolf, and C. S. Sloane, *J. Chem. Phys.* **71**, 2911 (1979).
7. W. L. Hase and D. G. Buckowski, *J. Comput. Chem.* **3**, 335 (1982).
8. W. L. Hase, D. Buckowskl, and K. N. Swamy, *J. Phys. Chem.* **87**, 2754 (1983).
9. K. N. Swamy and W. L. Hase, *J. Phys. Chem.* **87**, 4715 (1983).
10. W. L. Hase, H. B. Schlegel, V. Balbyshev, and M. Page, *J. Phys. Chem.* **100**, 5354 (1996).
11. J. Villà, A. González-Lafont, J. M. Lluch, and D. G. Truhlar, *J. Am. Chem. Soc.* **120**, 5559 (1998).
12. A. Sevin, H. T. Yu, and E. M. Evleth, *Journal of Molecular Structure: THEOCHEM* **104**, 163 (1983).
13. E. M. Evleth, H. Z. Cao, E. Kassab, and A. Sevin, *Chem. Phys. Lett.* **109**, 45 (1984).
14. A. S. Zyubin, A. M. Mebel, and S. H. Lin, *Chem. Phys. Lett.* **323**, 441 (2000).
15. J. L. Brum, S. Deshmukh, and B. Koplitz, *J. Chem. Phys.* **95**, 2200 (1991).
16. J. L. Brum, S. Deshmukh, Z. Wang, and B. Koplitz, *J. Chem. Phys.* **98**, 1178 (1993).
17. T. Gilbert, T. L. Grebner, I. Fischer, and P. Chen, *J. Chem. Phys.* **110**, 5485 (1999).
18. G. Amaral, K. Xu, and J. Zhang, *J. Chem. Phys.* **114**, 5164 (2001).

19. M. Zierhut, B. Noller, T. Schultz, and I. Fischer, *J. Chem. Phys.* **122**, 094302 (2005).

20. J. M. Hostettler, A. Bach, and P. Chen, *J. Chem. Phys.* **130**, 034303 (2009).

21. M. Steinbauer, J. Giegerich, K. H. Fischer, and I. Fischer, *J. Chem. Phys.* **137**, 014303 (2012).

22. S. Marggi Poullain, D. V. Chicharro, A. Zanchet, L. Rubio-Lago, A. García-Vela, and L. Bañares, *Phys Chem Chem Phys* **21**, 23017 (2019).

23. J. Munk, P. Pagsberg, E. Ratajczak, and A. Sillesen, *J. Phys. Chem.* **90**, 2752 (1986).

24. H. R. Wendt and H. E. Hunziker, *J. Chem. Phys.* **81**, 717 (1984).

25. K. Fagerström, A. Lund, G. Mahmoud, J. T. Jodkowski, and E. Ratajczak, *Chem. Phys. Lett.* **204**, 226 (1993).

26. B. H. Lengsfield, P. E. M. Siegbahn, and B. Liu, *J. Chem. Phys.* **81**, 710 (1984).

27. M. R. A. Blomberg and B. Liu, *J. Chem. Phys.* **83**, 3995 (1985).

28. B. Ruscic, *J. Phys. Chem. A* **119**, 7810 (2015).

29. M. T. Nguyen, M. H. Matus, W. A. Lester, and D. A. Dixon, *J. Phys. Chem. A* **112**, 2082 (2008).

30. B. Gemein and S. D. Peyerimhoff, *J. Phys. Chem.* **100**, 19257 (1996).

31. A. Bach, J. M. Hostettler, and P. Chen, *J. Chem. Phys.* **123**, 21101 (2005).

32. A. Bach, J. M. Hostettler, and P. Chen, *J. Chem. Phys.* **125**, 24304 (2006).

33. A. F. Wagner, L. A. Rivera-Rivera, D. Bachellerie, J. W. Perry, and D. L. Thompson, *J. Phys. Chem. A* **117**, 11624 (2013).

34. A. Matsugi, *J. Phys. Chem. Lett.* **4**, 4237 (2013).

35. K. Xu, G. Amaral, and J. Zhang, *J. Chem. Phys.* **111**, 6271 (1999).

36. M. Lucas, J. Minor, J. Zhang, and C. Brazier, *Chin. J. Chem. Phys.* **27**, 621 (2014).

37. Y. Song, X. Zheng, W. Zhou, M. Lucas, and J. Zhang, *J. Chem. Phys.* **142**, 224306 (2015).

38. G. Sun, Y. Song, and J. Zhang, *Chin. J. Chem. Phys.* **31**, 439 (2018).

39. Y. Song, M. Lucas, M. Alcaraz, J. Zhang, and C. Brazier, *The Journal of Physical Chemistry A* **119**, 12318 (2015).

40. S. Han, X. Zheng, S. Ndengué, Y. Song, R. Dawes, D. Xie, J. Zhang, and H. Guo, *Science Advances* **5**, eaau0582 (2019).

41. J. Zhang, M. Dulligan, and C. Wittig, *J. Phys. Chem.* **99**, 7446 (1995).

42. R. N. Zare, *Mol. Photochem.* **4**, 1 (1972).

43. J.-H. Wang, Y.-T. Hsu, and K. Liu, *J. Phys. Chem. A* **101**, 6593 (1997).

44. W. L. Smith and I. M. Mills, *J. Chem. Phys.* **40**, 2095 (1964).

45. W. Knippers, K. Van Helvoort, S. Stolte, and J. Reuss, *Chem. Phys.* **98**, 1 (1985).

46. J. L. Duncan and A. M. Ferguson, *J. Chem. Phys.* **89**, 4216 (1988).

47. J. L. Duncan and G. E. Robertson, *J. Mol. Spectrosc.* **145**, 251 (1991).

48. R. Georges, M. Bach, and M. Herman, *Mol. Phys.* **97**, 279 (1999).

49. M. D. Harmony, V. W. Laurie, R. L. Kuczkowski, R. H. Schwendeman, D. A. Ramsay, F. J. Lovas, W. J. Lafferty, and A. G. Maki, *J. Phys. Chem. Ref. Data* **8**, 619 (1979).

50. G. Sun, W. Zhou, X. Zheng, Y. Qin, Y. Song, Y. Yuan, and J. Zhang, *Molecular Physics* **119**, e1837974 (2021).

51. J. Brzozowski, P. Erman, and M. Lyyra, *Phys. Scr.* **17**, 507 (1978).

52. Y. Qin, X. Zheng, Y. Song, G. Sun, and J. Zhang, *The Journal of Chemical Physics* **157** (2022).

53. R. R. Friedl, W. H. Brune, and J. G. Anderson, *The Journal of Chemical Physics* **79**, 4227 (1983).

54. X. Wang, W. E. Turner, 2nd, J. Agarwal, and H. F. Schaefer, 3rd, *J. Phys. Chem. A* **118**, 7560 (2014).

55. M. T. Nguyen, M. H. Matus, W. A. Lester, and D. A. Dixon, *The Journal of Physical Chemistry A* **112**, 2082 (2008).

56. F. Qi, O. Sorkhabi, and A. G. Suits, *The Journal of Chemical Physics* **112**, 10707 (2000).

Figures and Captions

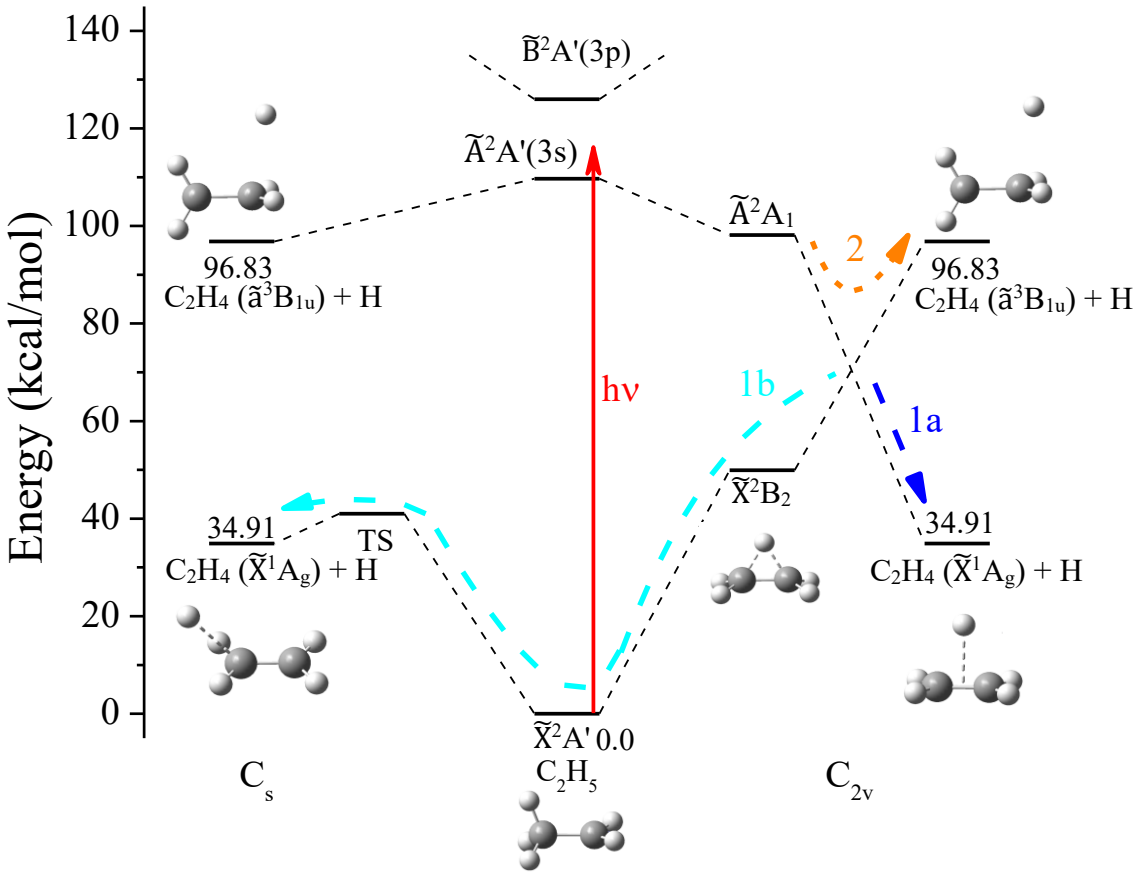

Figure 1. Potential energy diagram of the ethyl radical photodissociation system in C_s and C_{2v} symmetry. The energies of C_2H_5 [$\tilde{A}^2A'(3s)$] and C_2H_5 [$B^2A'(3p)$] in C_s are the estimated adiabatic excitation energies based on the UV absorption spectrum.[23-27] The energies of C_2H_5 ($\tilde{X}^2B_2$) and C_2H_5 ($\tilde{A}^2A_1$) in C_{2v} are based on Zyubin *et al.*'s theoretical calculation.[14] The blue arrow indicates prompt dissociation of C_2H_5 (3s) via the H-bridge configuration through the CI in C_{2v} geometry to the H + $C_2H_4(\tilde{X}^1A_g)$ products (Channel 1a). The light blue arrow represents unimolecular dissociation of the ground state ethyl radical to the H + $C_2H_4(\tilde{X}^1A_g)$ products after internal conversion from the 3s Rydberg state via the CI in C_{2v} geometry (Channel 1b). The orange arrow indicates the adiabatic dissociation of C_2H_5 (3s) via surface hopping to produce the H + triplet $C_2H_4(\tilde{a}^3B_{1u})$ products (Channel 2). See text for more details.

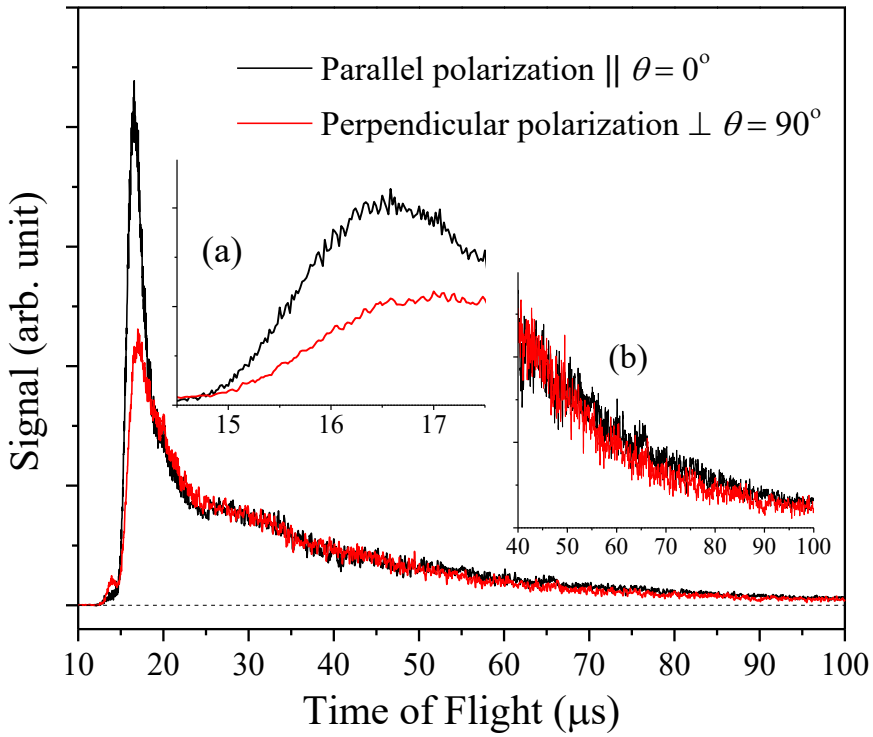

Figure 2. Net H-atom TOF spectra of 245 nm photodissociation of jet-cooled C_2H_5 (from 0.2% nitroethane precursor in 1000 Torr of Ar), with the electric vector of the linearly polarized photolysis radiation parallel (∥, $\theta = 0°$) and perpendicular (⊥, $\theta = 90°$) to the TOF path. The signals have been normalized to the same photolysis laser power and laser shots. The inset (a) shows partially resolved vibrational structure of the ethylene product in the region of 15-17 μs. The inset (b) shows a slightly higher intensity at the perpendicular (⊥) polarization in the region of 50-90 μs.

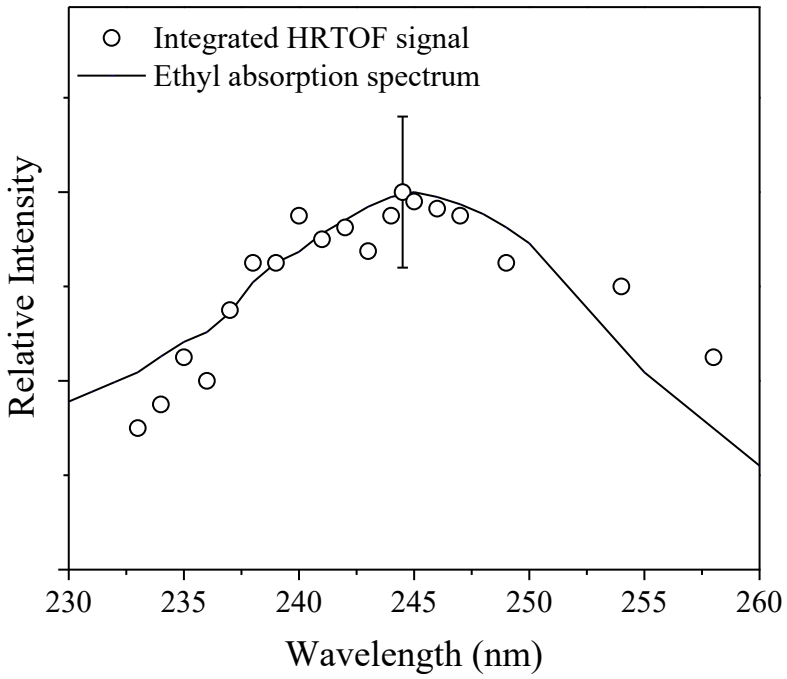

Figure 3. H-atom photofragment yield (PFY) spectrum as a function of photolysis wavelength in the region of 230-260 nm. The PFY (in open circles) was obtained by integrating the HRTOF signals at different photolysis excitation wavelength and was normalized with the photolysis laser power and number of shots. The error bar indicates 95% confidence limit based on multiple measurements at 245 nm. The solid line represents the absorption spectrum of ethyl taken from Fagerström et al.[25] Both the PFY and absorption spectrum were scaled to 1 at their maximum intensities.

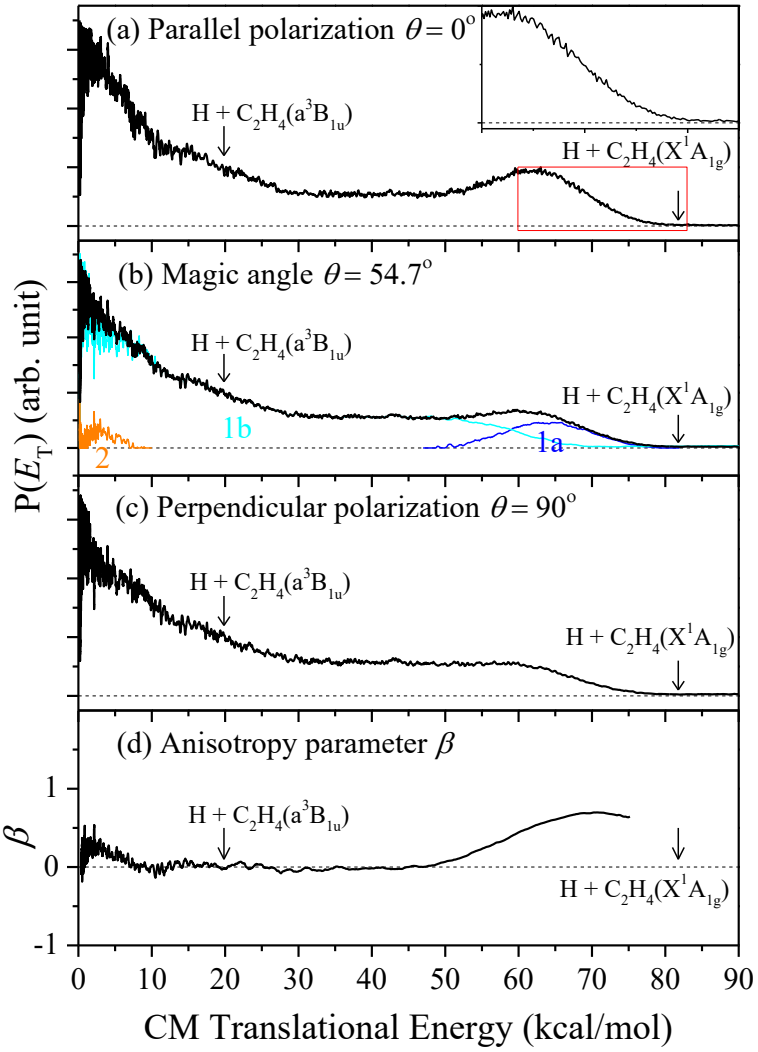

Figure 4. H + C_2H_4 products center-of-mass translational energy distribution $P(E_T, \theta)$ derived from the TOF spectra in Figure 2 at 245 nm photolysis wavelength. The polarization of the photolysis radiation is (a) parallel, (b) at the magic angle, and (c) perpendicular to the TOF path. (d) is the translational energy dependent anisotropy parameter $\beta(E_T)$. The magic angle distribution, $P_m(E_T)$, is deconvoluted into component 1a, 1b, and 2. The inset in (a) shows partially resolved vibrational structure of the ethylene product at $E_T > 60$ kcal/mol. The arrows indicate the maximum available energy of the H + $C_2H_4(\tilde{X}^1A_g)$ and H + $C_2H_4(\tilde{a}^3B_{1u})$ product channel, respectively. See text for more details.

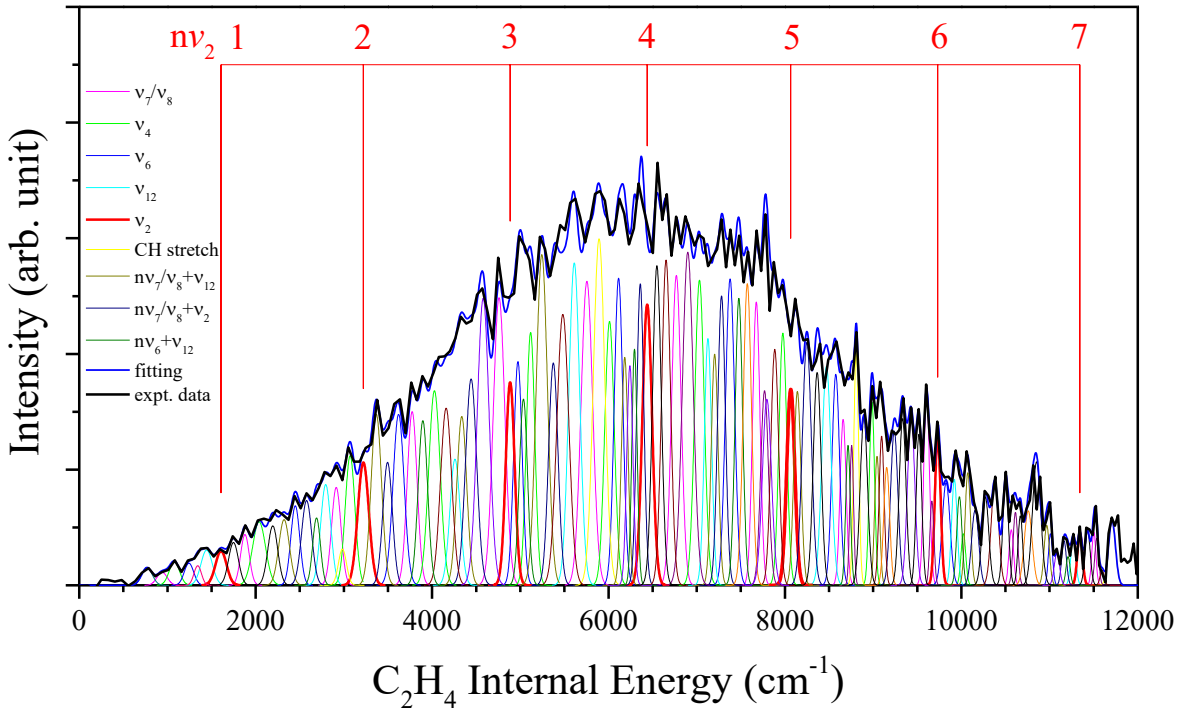

Figure 5. Internal energy distribution, $P_{1a}(E_{\mathrm{int}})$, of the $C_2H_4(\tilde{X}^1A_g)$ product in Channel 1a. The solid black line is the experimental distribution, and the solid blue line is the fitting/modeling using Gaussian peaks for vibrational levels of $C_2H_4(\tilde{X}^1A_g)$ (which are shown as narrow peaks in thin lines in various colors for different vibrational progressions). The fitting/modeling indicates that the vibrational peaks are mainly due to five pure vibrational mode progressions: ν_2, ν_4, ν_6, ν_7/ν_8, and ν_{12}, as well as combination mode progressions such as $\nu_7 + \nu_{12}$, $\nu_6 + \nu_{12}$, and $\nu_7 + \nu_2$. The C-C stretching ν_2 progression is highlighted by the Gaussian peaks in solid red line and is also indicated by the red comb lines. See text for more details.

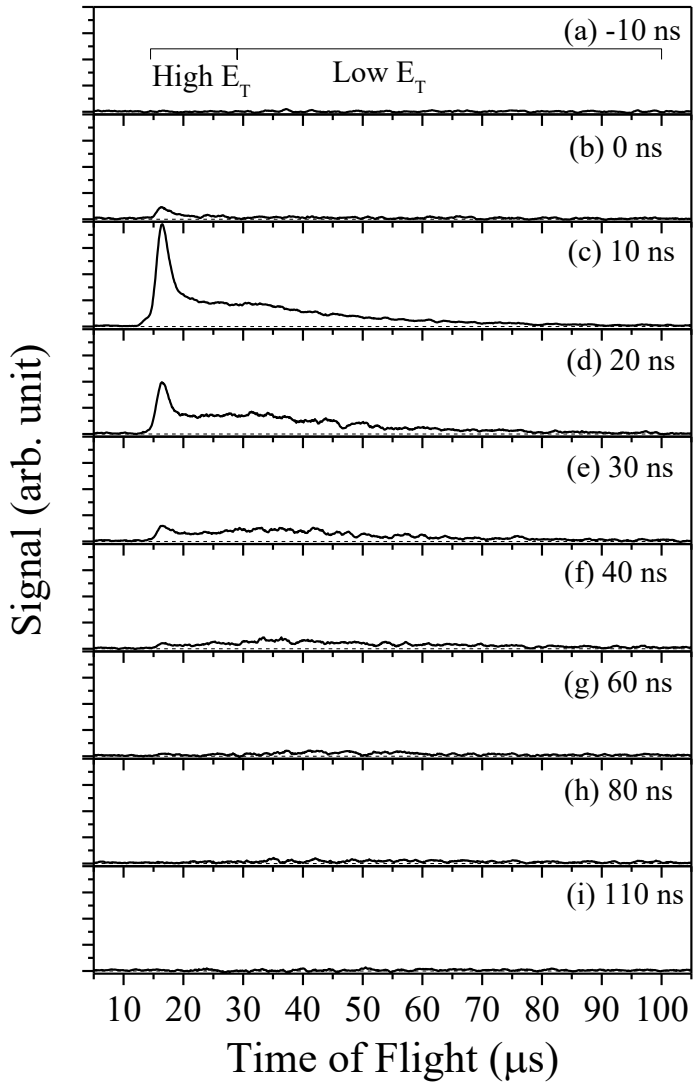

Figure 6. H-atom TOF spectra of 244 nm photodissociation of ethyl radical (nitroethane precursor) at different pump-probe delay time. All the spectra are normalized to the same laser power and number of shots. The photolysis laser polarization is parallel to the TOF path. The high E_T region is mainly for the fast H atoms from Channel 1a, and the low E_T region is mainly for the slow H atoms from Channel 1b.

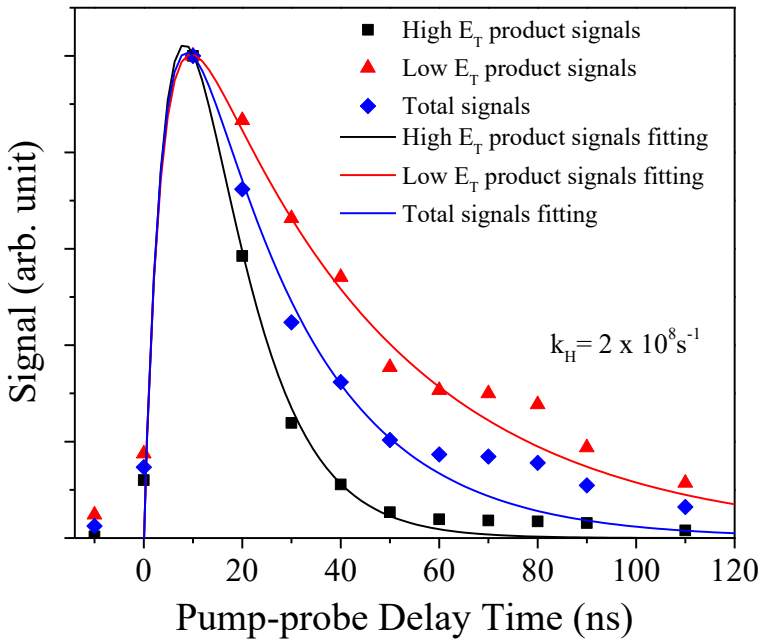

Figure 7. Integrated H-atom product signal from the photodissociation of ethyl radical (nitroethane precursor) as a function of photolysis and probe laser delay time. The signals were obtained by integrating the HRTOF spectra in different TOF regions (total, high E_T for fast H-atoms, and low E_T for slow H atoms, see Figure 6) as a function of pump-probe delay time. The signals were scaled to the maximum of each time profile. The solid lines are the fittings result of the H-atom product time profiles for obtaining the dissociation rate constant k_H (Ref. 17 and 39). See text for more details.

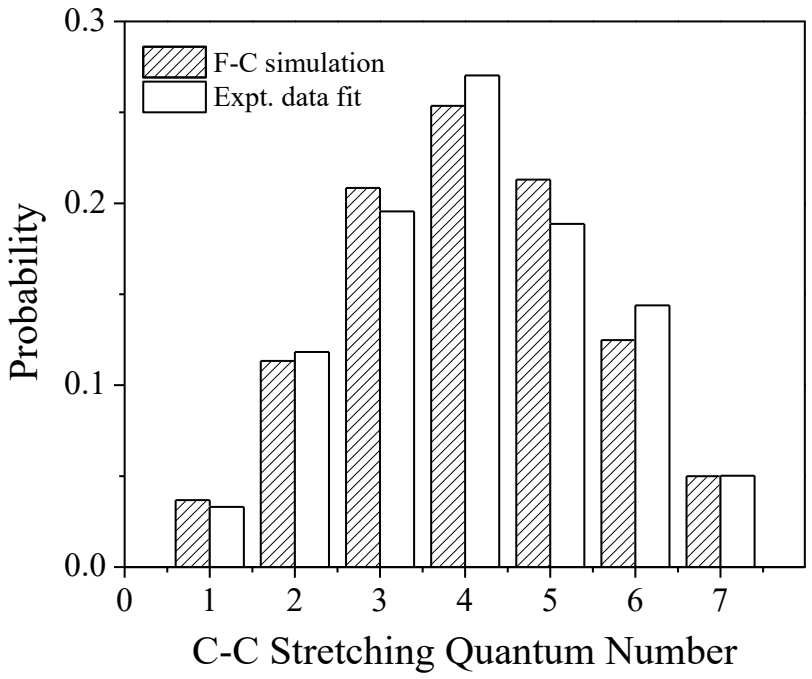

Figure 8. Vibrational state population of the C-C stretching (ν2) mode from Franck-Condon calculation and from peak fitting of the experimental P(E_{int}) distribution. The total population of the calculated and the experimental vibrational distributions are both normalized to 1. See text for more details.

Table 1. The $\langle E_T \rangle$, $\langle f_T \rangle$, β, and branching ratios of different dissociation channels.

	Channel 1a	Channel 1b	Channel 2
$\langle E_T \rangle$ (kcal/mol)	63.9	22.2	3.6
$\langle f_T \rangle$	0.78	0.27	0.18
β	0.67±0.10	0±0.10	0.25±0.10 to 2
branching ratio	0.11	0.87	0.02 (0.01 to 0.10)

Table 2. Main vibrational peak assignments of the $C_2H_4(\tilde{X}^1A_g)$ internal energy distribution in Channel 1a in Figure 5. Intensities and positions of the fitted vibrational peaks for the vibrationally excited $C_2H_4(\tilde{X}^1A_g)$ product are listed and organized by vibrational progressions. The vibrational modes are C-C stretching (ν_2), C-H stretching (ν_1, ν_5, ν_9, and ν_{11}), H-C-H in-plane bending (ν_3, ν_6, ν_{10}, and ν_{12}) and H-C-H out-of-plane bending (ν_4, ν_7, and ν_8). The vibrational frequencies and anharmonic parameters from Ref [48] are used to predict the peak positions.

peak assignment	relative intensity	peak position in cm^{-1}	peak assignment	relative intensity	peak position in cm^{-1}
ν_7/ν_8	0.11	939	ν_4	0.20	1078
$2\nu_7/\nu_8$	0.44	1878	$2\nu_4$	0.55	2038
$3\nu_7/\nu_8$	0.85	2914	$3\nu_4$	1.12	3070
$4\nu_7/\nu_8$	1.50	3774	$4\nu_4$	1.68	4027
$5\nu_7/\nu_8$	2.49	4759	$5\nu_4$	2.19	5117
$6\nu_7/\nu_8$	2.63	5755	$6\nu_4$	2.28	6011
$7\nu_7/\nu_8$	2.68	6769	$7\nu_4$	2.64	7031
$8\nu_7/\nu_8$	2.45	7676	$8\nu_4$	2.18	7977
$9\nu_7/\nu_8$	1.43	8660	$9\nu_4$	1.58	8986
$10\nu_7/\nu_8$	1.66	9606	$10\nu_4$	0.45	10023
$11\nu_7/\nu_8$	0.48	10566			
$12\nu_7/\nu_8$	0.46	11502	ν_6	0.19	1243
			$2\nu_6$	0.69	2449
ν_2	0.30	1607	$3\nu_6$	1.48	3620
$2\nu_2$	1.06	3220	$4\nu_6$	1.93	4973
$3\nu_2$	1.76	4885	$5\nu_6$	2.65	6114
$4\nu_2$	2.43	6439	$6\nu_6$	2.65	7378
$5\nu_2$	1.69	8066	$7\nu_6$	1.82	8576
$6\nu_2$	1.29	9732	$8\nu_6$	0.89	9827
$7\nu_2$	0.45	11344	$9\nu_6$	0.45	11010
ν_{12}	0.30	1444	$\nu_6+\nu_{12}$	0.58	2690
$2\nu_{12}$	0.87	2794	$2\nu_6+\nu_{12}$	1.42	3895
$3\nu_{12}$	1.09	4260	$3\nu_6+\nu_{12}$	1.61	5036
$4\nu_{12}$	2.79	5612	$4\nu_6+\nu_{12}$	2.04	6294
$5\nu_{12}$	2.13	7127	$5\nu_6+\nu_{12}$	2.48	7478
$6\nu_{12}$	1.89	8471	$6\nu_6+\nu_{12}$	1.21	8716
$7\nu_{12}$	0.91	9921	$7\nu_6+\nu_{12}$	0.77	9978
$8\nu_{12}$	0.41	11269	$8\nu_6+\nu_{12}$	0.25	11210

$\nu_7+\nu_2$	0.73	2577	$\nu_7+\nu_{12}$	0.57	2322
$2\nu_7+\nu_2$	1.06	3495	$2\nu_7+\nu_{12}$	1.48	3367
$3\nu_7+\nu_2$	1.78	4442	$3\nu_7+\nu_{12}$	1.46	4336
$4\nu_7+\nu_2$	1.92	5374	$4\nu_7+\nu_{12}$	2.86	5244
$5\nu_7+\nu_2$	2.61	6360	$5\nu_7+\nu_{12}$	1.97	6184
$6\nu_7+\nu_2$	2.50	7281	$6\nu_7+\nu_{12}$	2.00	7204
$7\nu_7+\nu_2$	2.10	8248	$7\nu_7+\nu_{12}$	1.68	8141
$8\nu_7+\nu_2$	1.33	9239	$8\nu_7+\nu_{12}$	1.15	9044
$9\nu_7+\nu_2$	0.65	10156	$9\nu_7+\nu_{12}$	0.97	10073
$10\nu_7+\nu_2$	0.38	11164	$10\nu_7+\nu_{12}$	0.52	10968